Macromolecules

Article

Cite This: Macromolecules 2019, 52, 1567−1576

pubs.acs.org/Macromolecules

Pronounced Surface Effects on the Curie Transition Temperature in Nanoconfined P(VDF-TrFE) Crystals

Niels L. Meereboer, Ivan Terzić, Harm Hendrik Mellema, Giuseppe Portale, and Katja Loos*

Macromolecular Chemistry and New Polymeric Materials, Zernike Institute for Advanced Materials, University of Groningen, Nijenborgh 4, 9747 AG Groningen, The Netherlands

Supporting Information

ABSTRACT: Changes in the Curie transition temperature of nanoconfined poly(vinylidene fluoride−trifluoroethylene) P(VDF-TrFE) copolymers can have a severe impact on the electroactive behavior and the application range of these materials. Therefore, the origin of the change in the Curie transition temperature requires a profound understanding. In this work, block copolymer self-assembly into a spherical morphology proves to be a viable method to effectively confine P(VDF-TrFE) in three dimensions for studying the effect of nanoconfinement on the Curie transition. Using differential scanning calorimetry and wide-angle X-ray scattering, easily accessible experimental techniques, we follow the crystalline phase transitions, showing that confining P(VDF-TrFE) in a nonpolar polystyrene (PS) or poly(4-*tert*-butoxystyrene) (P*t*BOS) matrix results in an increase of the Curie transition upon cooling and heating. However, when a more polar matrix is used to nanoconfine P(VDF-TrFE), the Curie transition temperature is drastically reduced due to surface effects.

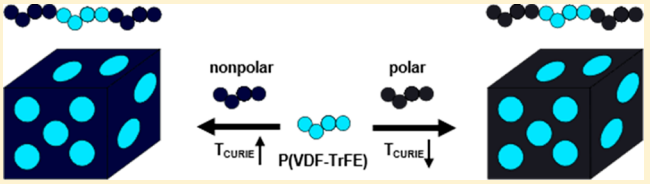

Ferroelectric polymers, like poly(vinylidene fluoride) (PVDF) and its copolymer with trifluoroethylene (P(VDF-TrFE)), are essential for the development of organic electronics, sensors, energy storage, and nonvolatile memory devices.[1−6] Especially, P(VDF-TrFE) has attracted great interest due to the ease of processing into the ferroelectric crystalline phase.[7,8] However, the ferroelectric properties of P(VDF-TrFE) rapidly deteriorate in the vicinity of the Curie transition temperature (T_{cr}), wherein a reversible ferroelectric-to-paraelectric crystalline phase transition is observed.[8,9] Nevertheless, a low T_{cr} is beneficial for other applications such as solid-state cooling devices and capacitive energy storage.[10,11] In solid-state cooling devices large changes in dipolar ordering under an applied electric field cause a jump in dielectric constant around the T_{cr}. This leads to an enormous electrocaloric effect when entropic energy is captured from the surroundings. Additionally, a jump in dielectric constant ensures an increased stored energy density inside dielectric materials. Therefore, a thorough understanding in how to tune the Curie transition temperature for a desired application is required (i.e., a high T_{cr} for ferroelectric applications and a low T_{cr} for capacitive energy storage and solid-state cooling devices).

The T_{cr} of P(VDF-TrFE) has been subjected to multiple studies including the effect of copolymer composition and crystallization temperature.[7,12,13] This phase transition is easily followed by differential scanning calorimetry (DSC), wide-angle X-ray scattering (WAXS) due to a change in crystalline phase, and Fourier transform infrared spectroscopy (FTIR) to identify the conformational isomers corresponding to the crystalline phases. It is found that the T_{cr} is mainly dependent on the crystallite size and the interplanar distance inside the crystals. Therefore, because of the bulkiness of the extra fluorine atom, increasing the TrFE content in the copolymers results in a reduction in the T_{cr}.[14] Furthermore, addition of a third copolymer, like chlorotrifluoroethylene, renders a (relaxor) ferroelectric terpolymer with a T_{cr} near room temperature due to an increase in the size of the crystal lattice, which reduces the energy barrier for the transition to occur.[15,16] Even though this crystalline phase transition in bulk materials is well explored, miniaturization of P(VDF-TrFE)-based materials down to the nanoscale may alter the crystallization mechanism and crystalline phase transitions drastically.

Recently, different top-down approaches have been performed to confine the crystallization of P(VDF-TrFE) in nanodomains. For example, Kassa et al. nanoimprinted P(VDF-TrFE) in the paraelectric phase (HTPE) to create free-standing nanopillars.[17] By measuring the ferroelectric contrast using piezoresponse force microscopy, they observed no significant changes in the Curie transition temperature probably due to the large ferroelectric domain size. Furthermore, since the first derivative of permittivity is proportional to the first derivative of density, the Russell group investigated the crystalline phase transitions using dielectric spectroscopy.[18,19] The high interfacial area between P(VDF-TrFE) and the polar aluminum oxide walls drastically influences the crystallization behavior. As a consequence of surface effects, the nanoconfined P(VDF-TrFE) shows a

Received: November 7, 2018
Revised: January 16, 2019
Published: February 6, 2019

DOI: 10.1021/acs.macromol.8b02382
Macromolecules 2019, 52, 1567−1576

Scheme 1. Synthetic Route toward PS-*b*-P(VDF-TrFE)-*b*-PS and P*t*BOS-*b*-P(VDF-TrFE)-*b*-P*t*BOS Triblock Copolymers

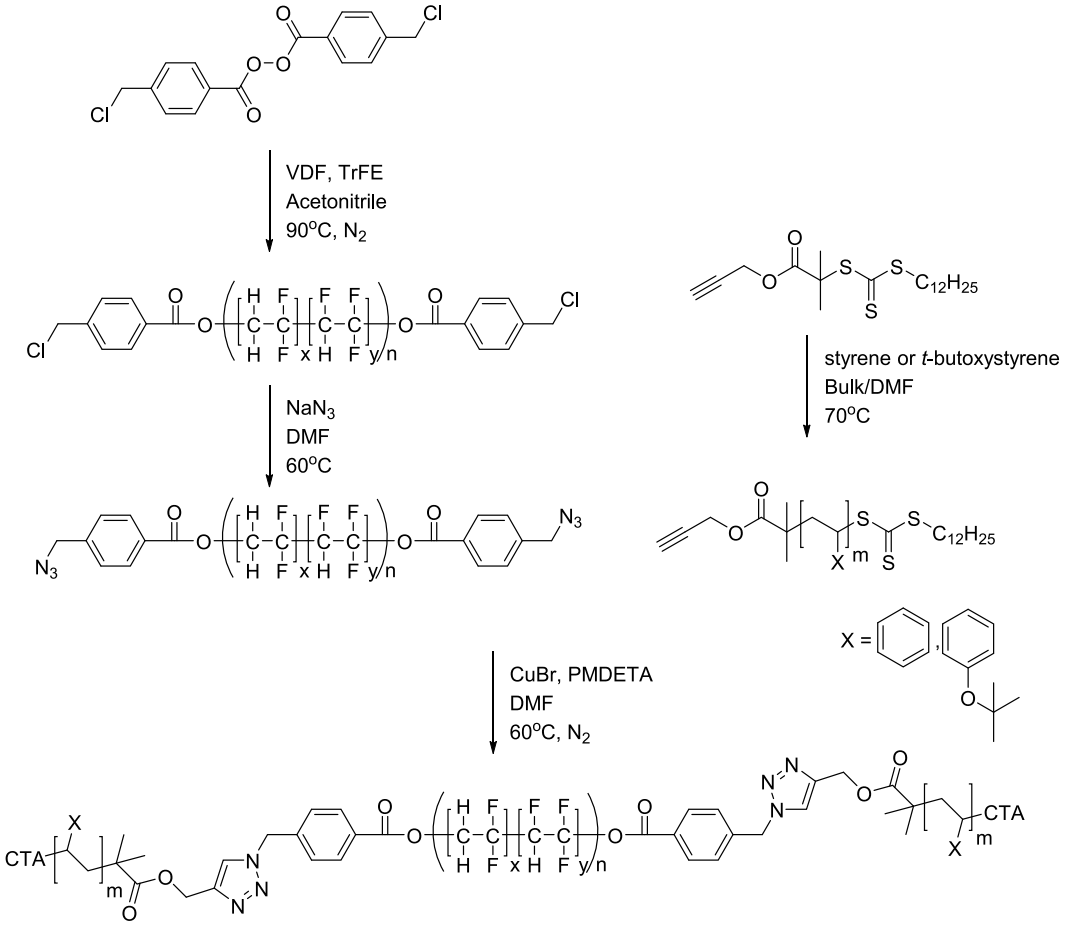

significantly lower Curie transition temperature. Although providing useful insights into the behavior of the Curie transition under nanoconfinement, the methods used for the determination of the T_{cr} are limited to their specific cases of confinement. Additionally, using top-down approaches only gives information about the effect of one- or two-dimensional confinement, whereas the size reduction effect on the T_{cr} under three-dimensional confinement is still unexplored.

Conversely, bottom-up approaches, such as block copolymer self-assembly, can enrich our understanding of the Curie transition temperature in three-dimensional nanoconfined space.[20] By use of a block copolymer approach, conventional experimental techniques for the characterization of bulk materials, like DSC and WAXS, can be used to examine the phase transitions.[13,21] Moreover, block polymers are a resourceful tool for crystallization studies in confined geometries due to the large diversity in nanodomain size, shape, hardness, or polarity by varying the molecular weight, block ratio, or physical properties (e.g., the glass transition temperature or polarity of the amorphous block), respectively.[21−24] Recently, we have shown that confined crystallization of PVDF in nanodomains is easily accessible via block copolymer self-assembly.[25−29] Consequently, when a spherical morphology is obtained, the crystallization behavior of PVDF drastically changes resulting in a homogeneous nucleation mechanism leading to a large undercooling and the formation of the thermodynamically favorable ferroelectric β-phase, demonstrating a strong effect of nanoconfinement on the crystallization using a block copolymer approach.[26]

In the current work, we investigate the impact of nanoconfinement on the Curie transition temperature inside P(VDF-TrFE)-based triblock copolymers using simple techniques such as WAXS and DSC. Besides the use of different TrFE contents in the P(VDF-TrFE) copolymers, the molecular structures of the amorphous matrix are carefully selected to obtain a hard confinement (high T_g) effect on the crystallization inside P(VDF-TrFE) nanospheres wherein the polarity of the surrounding matrix is increased *in situ*. This block copolymer approach allows us to exclusively study the effect of polarity on the T_{cr} next to the nanoconfinement effect, providing unique insights into aspects of the Curie transition inaccessible for top-down methods. Contrary to earlier observations, the confinement inside spherical nanodomains surrounded by a nonpolar matrix demonstrates an increase in the T_{cr} upon cooling. Additionally, an increasing polarity of the surrounding matrix significantly reduced the T_{cr} on both cooling and heating.

RESULTS AND DISCUSSION

Triblock Copolymer Synthesis. The synthetic route toward P(VDF-TrFE)-based triblock copolymers is outlined in Scheme 1. The chlorine functionalized benzoyl peroxide initiator is prepared according to the literature.[28] Subsequently, free radical copolymerization of VDF and TrFE is conducted, resulting in telechelic chlorine terminated P(VDF-TrFE) copolymers with molecular weights of 15.0 kg mol^{-1} and dispersity ($Đ$) around 1.4 (the molecular and structural characteristics of the polymers used in this study are

DOI: 10.1021/acs.macromol.8b02382
Macromolecules 2019, 52, 1567−1576

Table 1. Molecular Weight, Composition, and Structural Characteristics of the Synthesized (Block) Copolymers

polymer	M_n [a,f]	$Đ$ [b]	$w_{amorphous\ block}$ [c]	$w_{P(VDF\text{-}TrFE)}$ [c]	$v_{amorphous\ block}$ [d]	$v_{P(VDF\text{-}TrFE)}$ [d]	morphology	polar amorphous block
P(VDF_{82}-$TrFE_{18}$)[e]	15.6	1.46	0	1	0	1		
P(VDF_{72}-$TrFE_{28}$)[e]	14.8	1.28	0	1	0	1		
PS-*b*-P(VDF_{82}-$TrFE_{18}$)-*b*-PS	27.4[g]		0.43	0.57	0.56	0.44	spheres	no
PS-*b*-P(VDF_{72}-$TrFE_{28}$)-*b*-PS	23.9[g]		0.38	0.62	0.51	0.49	spheres	no
P*t*BOS-*b*-P(VDF_{72}-$TrFE_{28}$)-*b*-P*t*BOS	24.6[g]		0.40	0.60	0.54	0.46	spheres	no
PHS-*b*-P(VDF_{72}-$TrFE_{28}$)-*b*-PHS[h]	23.1[g]		0.36	0.64	0.47	0.53	spheres	yes

[a]Number-average molecular weight (M_n). [b]Dispersity ($Đ = M_w/M_n$). [c]The weight fractions were determined by ^{1}H NMR spectroscopy. [d]The volume fractions were calculated using the weight fractions and the density of PS (1.04 g cm^{-3}), P*t*BOS (1.00 g cm^{-3}), PHS (1.16 g cm^{-3}), and P(VDF-TrFE) (1.78 g cm^{-3}). [e]The P(VDF-TrFE) copolymers are designated according the molar ratio VDF and TrFE determined by ^{1}H NMR spectroscopy. [f]The molecular weight characteristics of P(VDF-TrFE) were calculated using GPC with DMF (0.01 M LiBr) as eluent and PMMA standards. [g]The block copolymer molecular weights were calculated using the M_n of P(VDF-TrFE) and weight fractions of the distinct blocks. [h]Molecular weight, composition, and morphology are obtained after in situ hydrolysis of P*t*BOS-*b*-P(VDF_{72}-$TrFE_{28}$)-*b*-P*t*BOS using trifluoroacetic acid.

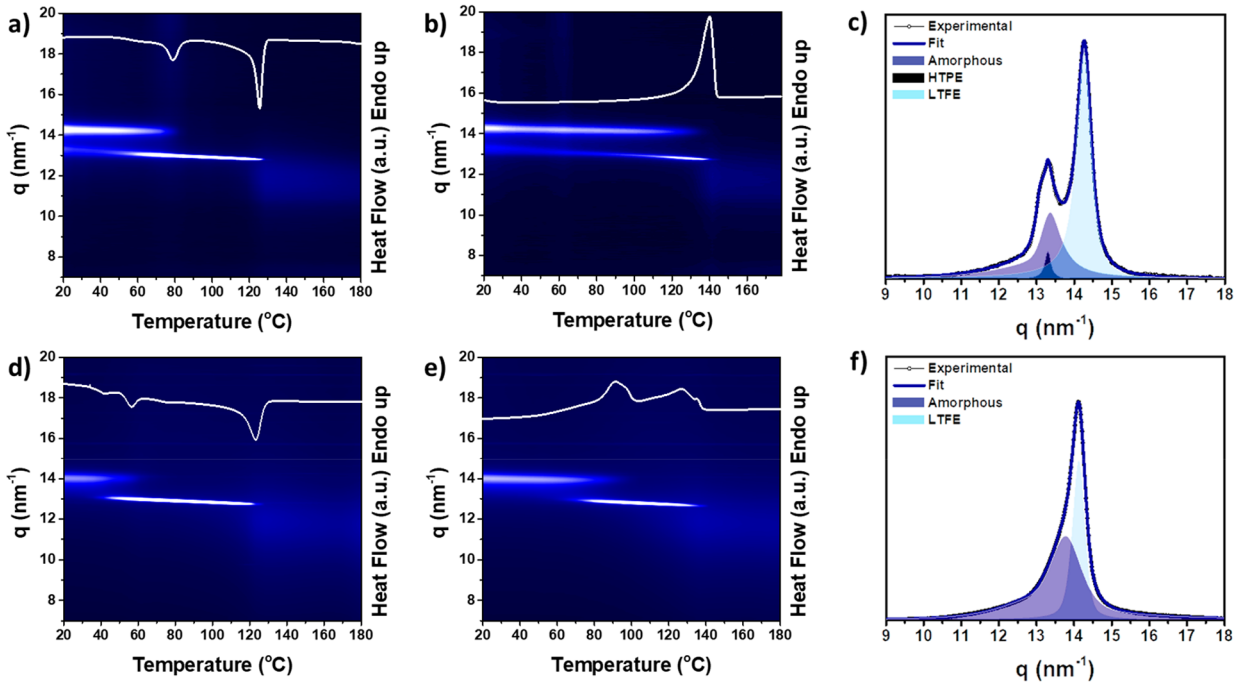

Figure 1. DSC and temperature-resolved WAXS profiles (2D surface plot) of P(VDF_{82}-$TrFE_{18}$) (a) cooled from the melt at 10 °C min^{-1}, (b) heated at 10 °C min^{-1}, and (c) the corresponding deconvoluted WAXS profile recorded at room temperature. DSC and temperature-resolved WAXS profiles of P(VDF_{72}-$TrFE_{28}$) (d) cooled from the melt at 10 °C min^{-1}, (e) heated at 10 °C min^{-1}, and (f) the corresponding deconvoluted WAXS profile recorded at room temperature. The WAXS profiles in the 2D surface plots are recorded over a 5 °C interval, wherein the surface represents the relative intensity.

summarized in Table 1). An end-group substitution was performed to fully convert the chlorine end groups into azide functionalities. Using ^{1}H NMR spectroscopy (Figure S1), we confirm the successful formation of the copolymer P(VDF-TrFE) with azide end-groups. Herein, the characteristic signals centered at 2.95 and 2.35 ppm demonstrate the presence of head-to-tail and tail-to-tail additions of VDF units, respectively, whereas the peaks corresponding to the proton from the TrFE units are located in between 5.00 and 5.50 ppm. In addition, the complete upfield shift of the singlet corresponding to the methylene proton next to the chlorine atom from 4.80 to 4.60 ppm shows the exchange of the end groups. The complementary polystyrene (PS) and poly(4-*tert*-butoxystyrene) (P*t*BOS) blocks with an alkyne functionality are synthesized using reversible addition−fragmentation chain transfer (RAFT) polymerization according to previous literature procedures.[28,30]

Subsequently, the highly efficient and quantitative CuAAC click reaction is used to prepare the PS-*b*-P(VDF-TrFE)-*b*-PS and P*t*BOS-*b*-P(VDF-TrFE)-*b*-P*t*BOS triblock copolymers. The ^{1}H NMR spectra show that the signal from the methylene proton next to the azide is fully shifted downfield, and additionally, the triazole proton appears at 7.90 ppm, demonstrating a successful click reaction. The gel permeation chromatography (GPC) elugrams, depicted in Figure S2, show a change of the negative P(VDF-TrFE) refractive index signal to a signal with a positive value for the block copolymer. In addition, the unimodal symmetrical shapes of the product elugrams at lower retention volumes compared to both P(VDF-TrFE) and the alkyne terminated homopolymers, PS and P*t*BOS, prove the formation of the triblock copolymers.

DOI: 10.1021/acs.macromol.8b02382
Macromolecules 2019, 52, 1567−1576

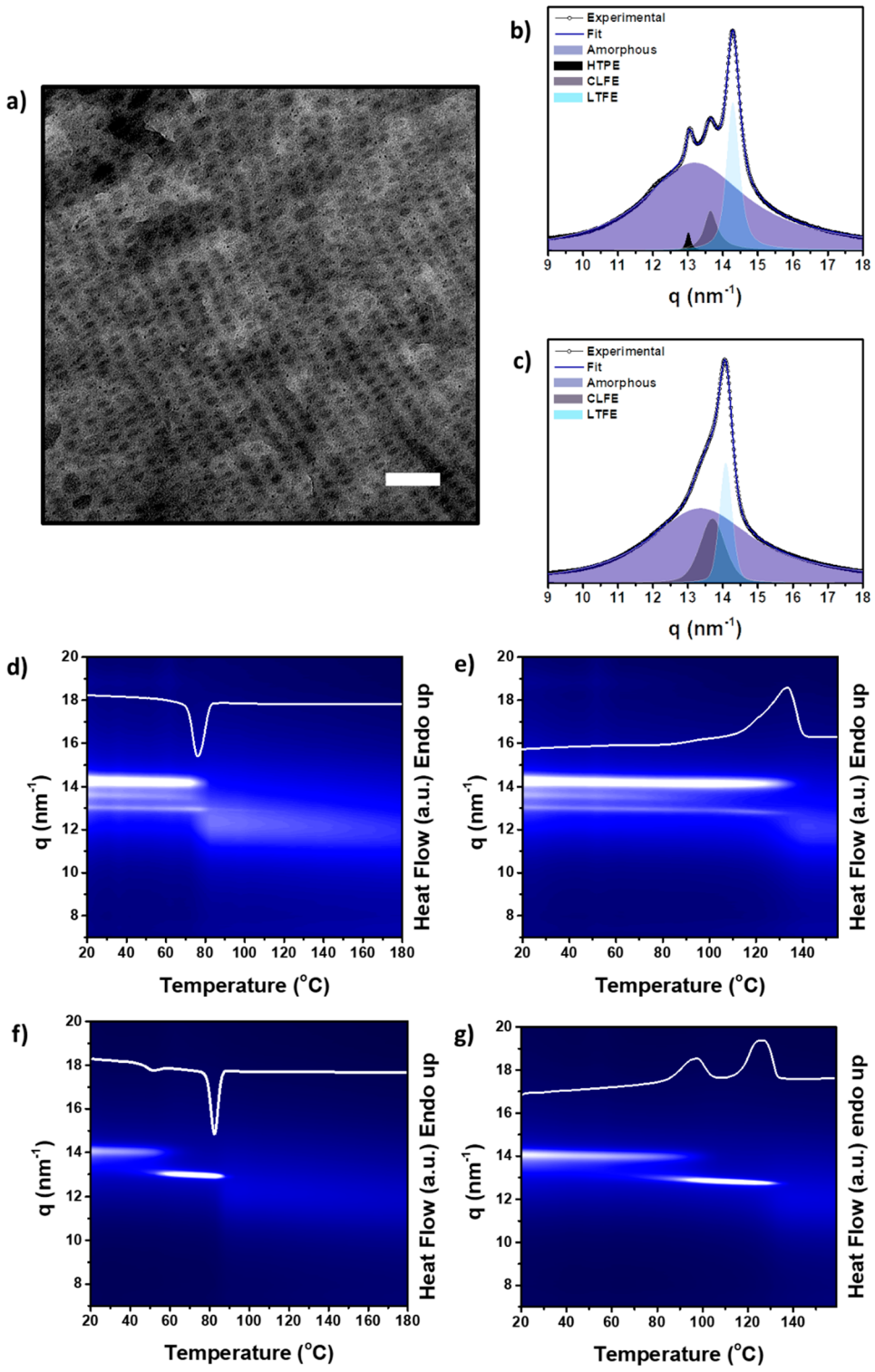

Figure 2. (a) TEM image of thermally annealed PS-*b*-P(VDF$_{82}$-TrFE$_{18}$)-*b*-PS recorded at room temperature. Scale bar corresponds to 100 nm. Deconvoluted WAXS profiles of (b) PS-*b*-P(VDF$_{82}$-TrFE$_{18}$)-*b*-PS and (c) PS-*b*-P(VDF$_{72}$-TrFE$_{28}$)-*b*-PS recorded at room temperature. DSC and temperature-resolved WAXS profiles (2D surface plot) of PS-*b*-P(VDF$_{82}$-TrFE$_{18}$)-*b*-PS (d) after cooling from the melt at 10 °C min^{-1} and (e) heating at 10 °C min^{-1}. DSC and temperature-resolved WAXS profiles (2D surface plot) of PS-*b*-P(VDF$_{72}$-TrFE$_{28}$)-*b*-PS (f) after cooling from the melt at 10 °C min^{-1} and (g) heating at 10 °C min^{-1}. The WAXS profiles in the 2D surface plots are recorded over a 5 °C interval, wherein the surface represents the relative intensity.

Curie Transition Temperature in P(VDF-TrFE) Copolymers. To understand the Curie transition temperature in the triblock copolymer films, we first analyzed the as-synthesized P(VDF-TrFE) copolymers used in this study. The P(VDF-TrFE) copolymers are designated according to their molar ratio VDF and TrFE (e.g., P(VDF$_{82}$-TrFE$_{18}$) contains 18 mol

DOI: 10.1021/acs.macromol.8b02382
Macromolecules 2019, 52, 1567−1576

% TrFE). The DSC profiles depicted in Figure 1 show that P(VDF_{82}-$TrFE_{18}$) has a slightly higher crystallization temperature than P(VDF_{72}-$TrFE_{28}$). Furthermore, the paraelectric-to-ferroelectric phase transition for P(VDF_{82}-$TrFE_{18}$) upon cooling is determined to be 75 °C (Figure 1a), whereas P(VDF_{72}-$TrFE_{28}$) shows two Curie transitions at 55 and 42 °C (Figure 1d). In the DSC heating scan there is no Curie transition detected when only 18 mol % TrFE is incorporated in the copolymer (Figure 1b). However, we observe a clear broad first-order temperature transition for P(VDF_{72}-$TrFE_{28}$) upon heating (Figure 1e). The Curie transition of P(VDF-TrFE) copolymers with varying TrFE content is well described in the literature.[14] The increased bulkiness of the TrFE units and the introduction of "defects" in the polymer backbone results in a lower crystallization temperature and a lower energy required for phase transitions to occur.

More information about the crystalline phase and phase transition is derived from the temperature-resolved WAXS profiles of the copolymers.[31,32] A 2D surface plot is chosen to visualize the crystallization and the Curie transition of the polymer samples, wherein the scattering vector (q) is plotted versus temperature (°C) having the relative intensities on the surface. Both copolymers first crystallize in the high-temperature paraelectric (HTPE) phase.[13] However, after the Curie transition, P(VDF_{82}-$TrFE_{18}$) demonstrates two distinct crystalline phases (HTPE and the low-temperature ferroelectric (LTFE)) at room temperature (Figure 1c), whereas P(VDF_{72}-$TrFE_{28}$) shows just the LTFE phases (Figure 1f). Because the low amount of TrFE inside P(VDF_{82}-$TrFE_{18}$) leads to small interplanar distances and therefore restricts chain mobility, a mixture of the ferroelectric and paraelectric phase is obtained upon cooling. Upon heating, the WAXS profiles of P(VDF_{82}-$TrFE_{18}$) reveal that the Curie transition and the melting endotherm coincide, although there is no phase transition observed for P(VDF_{82}-$TrFE_{18}$) in the DSC profile. For P(VDF_{72}-$TrFE_{28}$), the values of the T_{cr} and melting temperature are in good agreement in both WAXS and DSC.

Curie Transition under Nanoconfinement. For the effect of nanoconfinement on the T_{cr}, the block copolymers are designed to form spherical nanodomains of crystalline P(VDF-TrFE) inside an amorphous confining matrix. In this way, the crystallization occurs via a homogeneous nucleation mechanism, where surface effects on the crystallization are minimized due to unfavorable interaction between distinct blocks, resulting in chain stretching at the interface and crystallization inside the core of the spheres.[33] By use of block copolymers, wherein distinct block interactions are unfavorable, the mobility of the surrounding amorphous layer remains intact.

Two PS-*b*-P(VDF-TrFE)-*b*-PS triblock copolymers, PS-*b*-P(VDF_{82}-$TrFE_{18}$)-*b*-PS and PS-*b*-P(VDF_{72}-$TrFE_{28}$)-*b*-PS, giving a spherical morphology but with a different molar ratio VDF and TrFE, are selected for this study. The triblock copolymers are solvent-cast from dimethylformamide (DMF) at 45 °C. Subsequently, the films are thermally annealed in the melt followed by cooling to room temperature at a rate of 10 °C min^{-1}. The structure formation was identified using small-angle X-ray scattering (SAXS) and transmission electron microscopy (TEM). After thermal annealing in the melt and subsequent cooling to room temperature, disordered micellar spheres are formed in both PS-*b*-P(VDF-TrFE)-*b*-PS triblock copolymers as demonstrated in the TEM image (Figure 2a and Figure S3). Both PS-*b*-P(VDF-TrFE)-*b*-PS triblock copolymers show a first-order scattering maximum located at q = 0.15 nm^{-1} (Figure S4), indicating similar domains spacings. The lack of long-range periodicity, probably caused by the relatively high $Đ$ of the triblock copolymers and crystallization, is observed for various spherical micellar nanomorphologies in the literature.[34,35] Because of similar sphere diameters and since the same PS homopolymer was used for the click reaction, the effect of TrFE content in P(VDF-TrFE)-based block copolymers can effectively be studied.

As expected, a strongly reduced crystallization temperature for both PS-*b*-P(VDF-TrFE)-*b*-PS triblock copolymers is observed (Figure 2d,f). Recently, we noticed that nanoconfinement has a profound effect on the crystallization behavior of PVDF-based block copolymers.[26] Hard confinement in spherical nanodomains results in a strongly reduced crystallization temperature and the exclusive formation of the ferroelectric β-phase. In a similar way, because of a homogeneous nucleation mechanism, the crystallization temperature for PS-*b*-P(VDF_{82}-$TrFE_{18}$)-*b*-PS coincides with the T_{cr}. The deconvoluted WAXS profiles in Figure 2b show that P(VDF_{82}-$TrFE_{18}$) crystallizes inside the spherical nanodomains in a mixture of three crystalline phases. At 14.1 nm^{-1}, the characteristic (110/200) reflective plane signal corresponding to the LTFE phase appears, consisting out of all-trans organized P(VDF-TrFE) chains. The CLFE (cooled ferroelectric phase) is observed at 13.5 nm^{-1}, having trans sequences with gauche defects in the crystals, whereas the high-temperature HTPE phase is located at 13.1 nm^{-1}.

Bargain et al. already demonstrated the coexistence of the CLFE and the LTFE in P(VDF-TrFE) copolymers with high TrFE (>30 mol %) content.[13] However, the appearance of the CLFE is for the first time demonstrated in a copolymer with low TrFE content. Because of the increased surface area in spherical nanodomains, the mobility of the P(VDF-TrFE) chains at the boundary is strongly reduced, resulting in more gauche defects. In addition, the lower crystallization temperature favors the formation of crystals in the all-trans conformation but is hampered by the chain mobility, resulting in the CLFE. Upon heating the block copolymer, first the CLFE transforms to the HTPE before melting, whereas no transition of the ferroelectric phase is observed, probably due to the slightly lower melting temperature caused by the nanoconfinement effect.

The block copolymer with higher TrFE content, PS-*b*-P(VDF_{72}-$TrFE_{28}$)-*b*-PS, shows a crystallization temperature at 85 °C (Figure 2f), even though the same domains spacings were obtained from the TEM images and SAXS experiments. The higher TrFE content apparently favors the crystallization at higher temperature, since defects in the polymer backbone are functioning as nucleation points. As indicated by the WAXS profiles in Figure 2f, the higher crystallization temperature results in the crystallization into the kinetically favorable HTPE. Subsequently, the Curie transition to the LTFE is increased compared to pristine P(VDF_{72}-$TrFE_{28}$) (Figure S5). In addition, a CLFE next to the LTFE appears, indicating the reduced mobility of the P(VDF_{72}-$TrFE_{28}$) copolymer at the interface of the nanospheres. As the Curie transition is a consequence of cooperative movement of the polymer chains in the ferroelectric domain, the reduction in crystallite size results in smaller ferroelectric domains, leading to a lower energy barrier for the phase transition to occur. Indeed, as observed from the strong reduction of the enthalpy values for the Curie transition inside the block copolymers, crystallization inside spherical nanodomains results in a

DOI: 10.1021/acs.macromol.8b02382
Macromolecules 2019, 52, 1567−1576

reduction of ferroelectric domain size compared to pristine homopolymer.

Lutkenhaus et al. postulated that polar surfaces in contact with P(VDF-TrFE) may reduce the Curie transition in confined geometries with low feature sizes (15 nm).[19] To prove this, we designed a block copolymer system that phase separates in a spherical morphology with a polar matrix. However, the preparation of block copolymers that directly self-assemble into the desired morphology is difficult due to favorable interactions between the distinct blocks. Therefore, the desired system is prepared in two steps: microphase separation of P(VDF-TrFE) block copolymers using hydrolyzable nonpolar blocks with a high T_g into a spherical morphology followed by *in situ* hydrolysis to the polar matrix. Even though poly(alkyl methacrylates) are at first sight the most logical choice, their hydrolysis is accompanied by strong swelling due salt formation, which disrupts the morphology. The amorphous block that fulfilled all requirements (i.e., nanosphere formation, high T_g, and no swelling during hydrolysis) is poly(4-*tert*-butoxystyrene) (P*t*BOS).

The TEM image of P*t*BOS-*b*-P(VDF_{72}-$TrFE_{28}$)-*b*-P*t*BOS (Figure 3b) reveals that a disordered spherical nanomorphology is obtained after thermal annealing in the melt, with a first-order scattering maxima located at q = 0.22 nm^{-1}, as is observed for the PS-*b*-P(VDF-TrFE)-*b*-PS triblock copolymers. Even though the same P(VDF_{72}-$TrFE_{28}$) is used for the synthesis and a slightly higher molecular weight of P*t*BOS, the lower domain spacing might be a result of the washing step during the synthesis. In here, the selective solvent that removes unreacted homopolymer P*t*BOS can also extract a fraction of higher molecular weight P*t*BOS-*b*-P(VDF-TrFE)-*b*-P*t*BOS triblock copolymers, which leads to lower molecular weights. As expected, just as for PS-based triblock copolymers, higher-order peaks in the SAXS profiles are absent and the first-order scattering maxima remains at the same q-value upon cooling, indicating that the melt structure is retained at room temperature. Noteworthy, similar behavior regarding the Curie transition for P*t*BOS-*b*-P(VDF-TrFE)-*b*-P*t*BOS and the PS-based triblock copolymers is observed having in mind that P*t*BOS is also nonpolar.

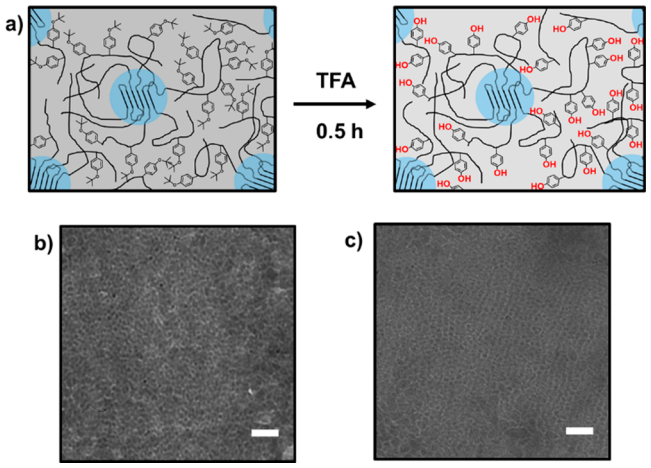

Figure 3. (a) Schematic representation of the *in situ* hydrolysis of thermally annealed P*t*BOS-*b*-P(VDF_{72}-$TrFE_{28}$)-*b*-P*t*BOS to PHS-*b*-P(VDF_{72}-$TrFE_{28}$)-*b*-PHS, increasing the polarity of the surrounding matrix of the P(VDF-TrFE) nanocrystals. (b) TEM image of thermally annealed P*t*BOS-*b*-P(VDF_{72}-$TrFE_{28}$)-*b*-P*t*BOS recorded at room temperature. Scale bar corresponds to 100 nm. (c) TEM image of *in situ* hydrolyzed PHS-*b*-P(VDF_{72}-$TrFE_{28}$)-*b*-PHS recorded at room temperature, showing that the structure is preserved. Scale bar corresponds to 100 nm.

To transfer P*t*BOS into a more polar matrix for the P(VDF-TrFE) nanospheres, the triblock copolymer films are hydrolyzed *in situ* with trifluoroacetic acid (TFA) to triblock copolymer films with a poly(4-hydroxystyrene) (PHS) matrix. As above mentioned, this leads to preservation of the nanospheres, since no swelling of the films occurred and P(VDF-TrFE) is insoluble in TFA. Indeed, removal of the *tert*-butyl protecting groups (Figure S1) demonstrates the successful hydrolysis process. Extensive drying (vacuum oven) and melting of the P(VDF-TrFE) crystals inside the PHS matrix at 150 °C indicate no significant changes in the morphology as observed in the SAXS profile and TEM image (Figure 3c), demonstrating that the spherical nanomorphology is retained after the hydrolysis step and thermal treatment. To prevent cross-linking and mixing of PHS and P(VDF-TrFE), the temperature is selected to be below the T_g of PHS (180 °C).[36]

The *in situ* hydrolyzed PHS-*b*-P(VDF-TrFE)-*b*-PHS triblock copolymer, similar to the PS- and P*t*BOS-based triblock copolymers, shows a large reduction in crystallization temperature due to crystallization in strongly confined spherical nanodomains. Intriguingly, as shown in Figure 4f, the HTPE phase is also observed at room temperature, which can be due to a reduced chain mobility at lower temperature, hampering the crystalline phase transition when cooling. Additionally, instead of a slight increase, a strong reduction in the T_{cr} is observed upon cooling. Subsequent heating leads to a reduced phase transition temperature compared to the P*t*BOS-*b*-P(VDF-TrFE)-*b*-P*t*BOS triblock copolymer. Because there are no large changes in the structure and the domain size (ΔH_{cr} values in Table S2) observed, the main cause for the reduction of the T_{cr} can be ascribed to polar interactions between P(VDF-TrFE) and PHS. The strong reduction in the T_{cr} (10 °C) has already been demonstrated in aluminum oxide nanopores.[19] Interactions of the surface with P(VDF-TrFE) reduced the Curie transition with 10 °C, whereas P(VDF-TrFE) further away from the interface showed similar behavior compared to the bulk material. By use of the same rationale, surface effects resulted in a near room temperature Curie transition in ultrathin films of the ferroelectric copolymer obtained via a Langmuir−Blodgett method, whereas the phase transition of the interior of the film is reduced with 10 °C.[37] The absence of two Curie transition in the block copolymers is a result of strong three-dimensional confinement.

To rationalize the change of the Curie transition temperature upon three-dimensional confinement, we should highlight the differences between neat P(VDF-TrFE) and the distinct block copolymers, including crystal size, crystallization mechanism, and interactions with P(VDF-TrFE) chains. Because the crystallization mechanism and temperature are similar regardless of the surrounding matrix, we can exclude these phenomena as driven force for the change of the Curie transition. Additionally, as indicated by the similar enthalpy values for the Curie transition (Table S2), the crystallite size of P(VDF-TrFE) in the distinct block copolymer systems is comparable, but completely different behavior is observed for the distinct block copolymers. Because for the crystalline phase transition of small sized P(VDF-TrFE) crystals no large displacement of the polymer chains is required, the Curie

DOI: 10.1021/acs.macromol.8b02382
Macromolecules 2019, 52, 1567−1576

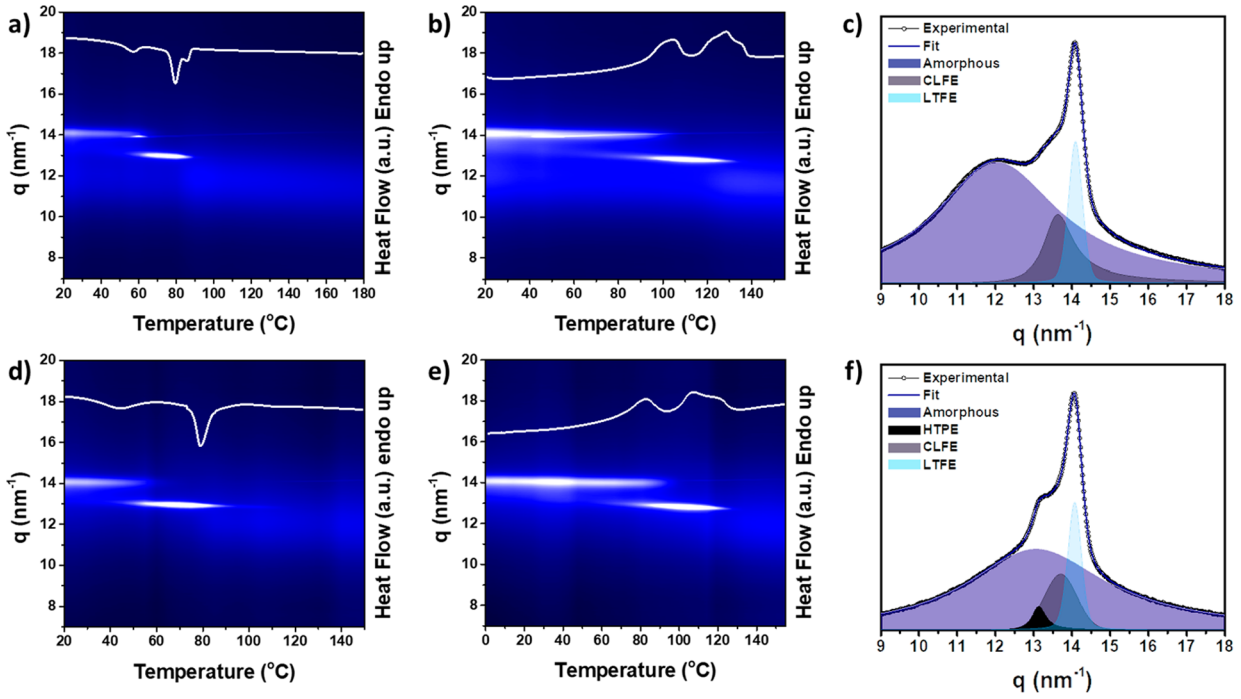

Figure 4. (a) DSC profile and WAXS surface plot from P*t*BOS-*b*-P(VDF$_{72}$-TrFE$_{28}$)-*b*-P*t*BOS cooled from the melt at 10 °C min^{-1}. (b) DSC profile and WAXS surface plot from P*t*BOS-*b*-P(VDF$_{72}$-TrFE$_{28}$)-*b*-P*t*BOS heated at 10 °C min^{-1}. (c) The corresponding deconvoluted WAXS profile of P*t*BOS-*b*-P(VDF$_{72}$-TrFE$_{28}$)-*b*-P*t*BOS recorded at room temperature when cooled from the melt. (d) DSC profile and WAXS surface plot from *in situ* hydrolyzed PHS-*b*-P(VDF$_{72}$-TrFE$_{28}$)-*b*-PHS cooled from 150 °C at 10 °C min^{-1}. (e) DSC profile and WAXS surface plot from *in situ* hydrolyzed PHS-*b*-P(VDF$_{72}$-TrFE$_{28}$)-*b*-PHS heated at 10 °C min^{-1}. (f) The corresponding deconvoluted WAXS profile of *in situ* hydrolyzed PHS-*b*-P(VDF$_{72}$-TrFE$_{28}$)-*b*-PHS recorded at room temperature when cooled from 150 °C. The WAXS profiles in the 2D surface plots are recorded over a 5 °C interval, wherein the surface represents the relative intensity.

transition temperature is increased.[38] However, taking into account the large number of hydroxyl groups in PHS and the possibility to form hydrogen-bonding interactions with P(VDF-TrFE) as is generally accepted in the literature, we relate the reduction of the Curie transition temperature to hydrogen bond formation between amorphous P(VDF-TrFE) chains and PHS.[39−43] Here, the hydrogen bond formation is described as interactions between the fluorine atoms and the hydroxyl groups. Because during the Curie transition cooperative motion of the polymer chains takes place, but the chain mobility of amorphous P(VDF-TrFE) is hampered due to hydrogen bond interactions, the Curie transition is reduced to lower temperatures.[38] Future work should provide deeper insights into morphological and crystallite size effects.

CONCLUSIONS

In summary, we elucidate the effect of the surrounding matrix and nanoconfinement on the Curie transition when P(VDF-TrFE) is confined in spherical nanodomains. Therefore, P(VDF-TrFE)-based triblock copolymer are designed to have a hard confinement effect on the crystallization with the possibility to tune the polarity of the amorphous block *in situ*. Using easy accessible experimental techniques, such as DSC and WAXS, we followed the crystalline-to-crystalline phase transitions, showing the power of block copolymers for fundamental studies. When a nonpolar matrix is used, a slight increase in the Curie transition is observed as a result of the crystallite size reduction. In contrast, a switch to a more polar surrounding strongly affected the T_{cr}. Polar interactions at the crystalline−amorphous interface lead to a strong reduction in the Curie transition temperature due to a reduced mobility of the polymer chains. Therefore, when confining P(VDF-TrFE) to finite nanodimensions, careful considerations have to be made to select the polarity of the surrounding matrix. In addition, to tune the T_{cr} for the desired application, block copolymers prove to be an appealing candidate due to the large variety in polymer blocks available.

METHODS

Materials. 2,2′-Azobis(2-methylpropionitrile) (AIBN, Fluka, 98+ %) was recrystallized twice from methanol. Copper(I) bromide (CuBr, Sigma-Aldrich, 98%) was stirred for 1 h in glacial acetic acid and then filtered and washed with ethanol and diethyl ether before drying under vacuum. 4-(Chloromethyl)benzoyl peroxide, 2-(dodecylthiocarbonothioylthio)-2-methylpropionic acid propargyl ester (RAFT agent), and the polystyrene (PS) and poly(4-*tert*-butoxystyrene) (P*t*BOS) homopolymers were prepared according to literature procedures.[28,44] Vinylidene fluoride (VDF, Synquest Laboratories, 98%), trifluoroethylene (TrFE, Synquest Laboratories, 98%), 1,1,4,7,7-pentamethyldiethylenetriamine (PMDETA, Acros Organics, 99+%), *N*,*N*-dimethylformamide (DMF, Acros Organics, anhydrous, 99.8%), and trifluoroacetic acid (TFA, Acros Organics, 99%) were used as received. All other solvents were analytical grade.

Synthesis of Chlorine-Terminated P(VDF-TrFE). A solution of 4-(chloromethyl)benzoyl peroxide (500 mg, 1.47 mmol) in 300 mL of anhydrous acetonitrile was introduced in a 600 mL Parr (model 4568) high-pressure reactor and purged with N_2 for 30 min. Subsequently, 2.2 bar (3.8 bar for 28 mol % TrFE) of TrFE followed by the addition of VDF until 20 bar (15 bar for 28 mol % TrFE) was introduced into the reactor at room temperature. The temperature inside the reactor was increased to 90 °C, and the reaction mixture was stirred at 500 rpm for an additional 30 min. The reactor was cooled by water to room temperature and depressurized to remove unreacted monomer. The solvent was removed *in vacuo*, and the remaining solid was washed multiple times with DCM to remove

DOI: 10.1021/acs.macromol.8b02382
Macromolecules 2019, 52, 1567−1576

initiator residues. The polymers were dried *in vacuo* at room temperature to obtain a light-yellow product. ^{1}H NMR (400 MHz, acetone-d_6): δ (ppm) = 8.09 (d, −ArH), 7.68 (d, −ArH), 6.10−5.12 (m, $-CHCF_2-$), 4.68 (m, $-COOCH_2CF_2-$), 4.60 (s, $-PhCH_2N_3$), 3.10−2.70 (m, $-CF_2CH_2-CF_2CH_2-$, head-to-tail), 2.40−2.20 (m, $-CF_2CH_2-CH_2CF_2-$, tail-to-tail).

Synthesis of Azide-Terminated P(VDF-TrFE). Chlorine-terminated P(VDF-TrFE) and sodium azide were dissolved in DMF and stirred overnight at 60 °C. The next day, the polymer solution was concentrated and precipitated in MeOH:H_2O (1:1) followed by extensive washing with H_2O. Subsequent drying *in vacuo* yielded the azide-terminated P(VDF-TrFE) copolymers. ^{1}H NMR (400 MHz, acetone-d_6): δ (ppm) = 8.11 (d, −ArH), 7.58 (d, −ArH), 6.10−5.12 (m, $-CHCF_2-$), 4.72 (m, $-COOCH_2CF_2-$), 4.81 (s, $-PhCH_2Cl$), 3.10−2.70 (m, $-CF_2CH_2-CF_2CH_2-$, head-to-tail), 2.40−2.20 (m, $-CF_2CH_2-CH_2CF_2-$, tail-to-tail).

Synthesis of PS-*b*-P(VDF-TrFE)-*b*-PS and P*t*BOS-*b*-P(VDF-TrFE)-*b*-P*t*BOS Triblock Copolymers. A general route for the Cu(I)-catalyzed alkyne azide cycloaddition (CuAAC) used for the preparation of block copolymers is described below. The alkyne-terminated P(VDF-TrFE) (300 mg, 0.025 mmol), PS (P*t*BOS), and CuBr were added into a predried Schlenk tube in a molar ratio [P(VDF-TrFE)]:[PS]:[CuBr] = 1:2.6:4. After performing degassing procedures (three repetitive cycles of evacuating and backfilling with N_2), 4 mL of anhydrous DMF was added, followed by PMDETA (30 μL, 0.14 mmol). The reaction was allowed to stir for 3 days at 60 °C and afterward stopped by exposing to the air. Residual copper catalyst was removed by passing the reaction mixture through a short neutral alumina column with THF as eluent. The solvents were removed *in vacuo*, and the mixture was dissolved in THF again. The polymers were precipitated in MeOH:H_2O (1:1). After filtration the product was collected via filtration, and the unreacted homopolymer was washed away with diethyl ether (*n*-hexanes for P*t*BOS) followed by centrifugation (5 min, 4500 rpm). The polymers were precipitated from DMF in MeOH:H_2O (2:3) once more to obtain a light brown powder. Finally, the block copolymers were dried *in vacuo*. ^{1}H NMR (400 MHz, acetone-d_6, PS-*b*-P(VDF-TrFE)-*b*-PS): δ (ppm) = 8.05 (d, −ArH), 7.89 (s, triazole), 7.45 (−ArH), 7.40−6.40 (−ArH, PS) 6.10−5.12 (m, $-CHCF_2-$), 4.72 (m, $-COOCH_2CF_2-$), 4.81 (s, $-PhCH_2Cl$), 3.10−2.70 (m, $-CF_2CH_2-CF_2CH_2-$, head-to-tail), 2.40−2.20 (m, $-CF_2CH_2-CH_2CF_2-$, tail-to-tail), 2.18−1.40 ($-CH_2CH(Ar)-$, PS). ^{1}H NMR (400 MHz, acetone-d_6, P*t*BOS-*b*-P(VDF-TrFE)-*b*-P*t*BOS): δ (ppm) = 8.05 (d, −ArH), 7.89 (s, triazole), 7.45 (−ArH), 6.90−6.00 (−ArH, P*t*BOS) 6.10−5.12 (m, $-CHCF_2-$), 4.72 (m, $-COOCH_2CF_2-$), 4.81 (s, $-PhCH_2Cl$), 3.10−2.70 (m, $-CF_2CH_2-CF_2CH_2-$, head-to-tail), 2.40−2.20 (m, $-CF_2CH_2-CH_2CF_2-$, tail-to-tail), 2.20−1.20 ($-CH_2CH(Ar)-$ and $-(CH_3)_3$, P*t*BOS).

Block Copolymer Film Formation. All the block copolymers, PS-*b*-P(VDF-TrFE)-*b*-PS and P*t*BOS-*b*-P(VDF_{72}-$TrFE_{28}$)-*b*-P*t*BOS, were dissolved in 4 mL of DMF (10 mg mL^{-1}). The solution was filtered over a 0.45 μm PTFE filter and subsequently poured in a glass Petri dish. The solvent was allowed to evaporate at 45 °C over 2 days. To obtain the spherical nanomorphology, the block copolymer films were heated to 180 °C at 10 °C min^{-1}, thermally annealed for 5 min at 180 °C, and subsequently cooled to room temperature at 10 °C min^{-1}. The thermally annealed P*t*BOS-*b*-P(VDF_{72}-$TrFE_{28}$)-*b*-P*t*BOS triblock copolymer films were *in situ* hydrolyzed to PHS-*b*-P(VDF_{72}-$TrFE_{28}$)-*b*-PHS by soaking into TFA for 30 min. The films were extensively rinsed with H_2O afterward and finally dried *in vacuo* at room temperature. After drying, PHS-*b*-P(VDF_{72}-$TrFE_{28}$)-*b*-PHS was subjected to the following temperature profile; heating to 150 °C, isothermal for 1 min, cooling to room temperature, and a final heating process to the melt. The rate was set at 10 °C min^{-1}.

Nuclear Magnetic Resonance (^{1}H NMR). ^{1}H NMR spectra were recorded on a 400 MHz Varian (VXR) spectrometer at room temperature.

Gel Permeation Chromatography (GPC). GPC of P(VDF-TrFE) copolymers and the P(VDF-TrFE)-based block copolymers was performed in DMF (containing 0.01 M LiBr) using a Viscotek GPCmax equipped with model 302 TDA detectors and two columns (Agilent Technologies-PolarGel-L and M, 8 μm 30 cm) at a flow rate of 1.0 mL min^{-1} and 50 °C. Narrow dispersity PMMA standards (Polymer Laboratories) were used for constructing an universal calibration curve applied for determining molecular weights of P(VDF-TrFE) and P*t*BOS. A triple detection method with THF, stabilized with BHT, as eluent and a flow rate of 1.0 mL min^{-1} at 35 °C was used to determine the molecular weight and the dispersity($Đ$) of PS. The separation was performed by utilizing two PL gel 5 μm MIXED-C, 300 mm columns (Agilent Technologies) calibrated with narrow dispersity polystyrene standards (Agilent Technologies and Polymer Laboratories). A predetermined refractive index increment (dn/dc) of 0.185 mL g^{-1} was used to calculate the molecular weight characteristics for PS.

Differential Scanning Calorimetry (DSC). DSC thermograms were recorded on a TA Instruments DSC Q1000 using heating and cooling rates of 10 °C min^{-1}.

In Situ X-ray Scattering. Temperature-resolved small-angle X-ray scattering and wide-angle X-ray scattering (SAXS and WAXS) measurements were performed at beamline BM26B at the European Synchrotron Radiation Facility (ESRF) in Grenoble with a wavelength λ = 0.97 Å.[31,32] Acquisition of simultaneously SAXS and WAXS patterns was performed over time intervals of 30 s using a Pilatus 1M detector (981 × 1043 pixels of 172 μm × 172 μm placed at a distance of 3.5 m) and a Pilatus 300K detector (1472 × 195 pixels of 172 μm × 172 μm placed at a distance of 0.28 m), respectively. The scattering vector q is defined as $q = 4\pi/\lambda(\sin\theta)$ with 2θ being the scattering angle. Temperature-resolved measurements were performed using a Linkam DSC 600 cell. The cooling and heating rate were set at 10 °C min^{-1}, resulting in a WAXS/SAXS profile every 5 °C. The temperature-resolved WAXS profiles are depicted as a 2D surface plot having the scattering vector q on the vertical axis and temperature on the horizontal axis; the surface represents the relative intensities of the WAXS profiles. Deconvolution of the WAXS profiles was achieved using a MATLAB script taking the WAXS profile recorded at room temperature. The experimental profiles were deconvoluted by using the sum of a linear background and pseudo-Voigt peaks describing the scattering from the amorphous and the crystalline phases.

Transmission Electron Microscopy (TEM). TEM was performed on a Philips CM12 transmission electron microscope operating at an accelerating voltage of 120 kV. A section of the thermally annealed (DSC) block copolymer film was embedded in epoxy resin (Epofix, Electron Microscopy Sciences) and subsequently microtomed using a Leica Ultracut UCT-ultramicrotome to prepare ultrathin sections (ca. 80 nm). No additional staining of the samples was required.

■ ASSOCIATED CONTENT

Supporting Information

The Supporting Information is available free of charge on the ACS Publications website at DOI: 10.1021/acs.macromol.8b02382.

^{1}H NMR spectra, GPC eluograms, SAXS profiles, and TEM image (PDF)

■ AUTHOR INFORMATION

Corresponding Author

*Tel +31-50 363 6867; e-mail k.u.loos@rug.nl.

ORCID

Giuseppe Portale: 0000-0002-4903-3159

Katja Loos: 0000-0002-4613-1159

Author Contributions

N.L.M. and I.T. contributed equally.

Notes

The authors declare no competing financial interest.

DOI: 10.1021/acs.macromol.8b02382
Macromolecules 2019, 52, 1567−1576

■ ACKNOWLEDGMENTS

The research was supported by an NWO-VICI innovational research grant. A. J. J. Woortman is acknowledged for the GPC measurements.

■ REFERENCES

(1) Soulestin, T.; Ladmiral, V.; Dos Santos, F. D.; Améduri, B. Vinylidene Fluoride- and Trifluoroethylene-Containing Fluorinated Electroactive Copolymers. How Does Chemistry Impact Properties? *Prog. Polym. Sci.* **2017**, *72*, 16−60.
(2) Chen, X.; Han, X.; Shen, Q.-D. PVDF-Based Ferroelectric Polymers in Modern Flexible Electronics. *Adv.Electron. Mater.* **2017**, *3*, 1600460.
(3) Hu, Z.; Tian, M.; Nysten, B.; Jonas, A. M. Regular Arrays of Highly Ordered Ferroelectric Polymer Nanostructures for Non-Volatile Low-Voltage Memories. *Nat. Mater.* **2009**, *8*, 62−67.
(4) Lee, J.-H.; Lee, K. Y.; Kumar, B.; Tien, N. T.; Lee, N.-E.; Kim, S.-W. Highly Sensitive Stretchable Transparent Piezoelectric Nanogenerators. *Energy Environ. Sci.* **2013**, *6*, 169−175.
(5) Khanchaitit, P.; Han, K.; Gadinski, M. R.; Li, Q.; Wang, Q. Ferroelectric Polymer Networks with High Energy Density and Improved Discharged Efficiency for Dielectric Energy Storage. *Nat. Commun.* **2013**, *4*, 2845.
(6) Zhang, Q. M.; Bharti, V.; Zhao, X. Giant Electrostriction and Relaxor Ferroelectric Behavior in Electron-Irradiated Poly(Vinylidene Fluoride-Trifluoroethylene) Copolymer. *Science* **1998**, *280*, 2101−2104.
(7) Tashiro, K.; Takano, K.; Kobayashi, M.; Chatani, Y.; Tadokoro, H. Structural Study on Ferroelectric Phase Transition of Vinylidene Fluoride-Trifluoroethylene Copolymers (III) Dependence of Transitional Behavior on VDF Molar Content. *Ferroelectrics* **1984**, *57*, 297−326.
(8) Furukawa, T. Structure and Functional Properties of Ferroelectric Polymers. *Adv. Colloid Interface Sci.* **1997**, *71*−*72*, 183−208.
(9) Furukawa, T.; Date, M.; Fukada, E.; Tajitsu, Y.; Chiba, A. Ferroelectric Behavior in the Copolymer of Vinylidenefluoride and Trifluoroethylene. *Jpn. J. Appl. Phys.* **1980**, *19*, L109.
(10) Neese, B.; Chu, B.; Lu, S.-G.; Wang, Y.; Furman, E.; Zhang, Q. M. Large Electrocaloric Effect in Ferroelectric Polymers Near Room Temperature. *Science* **2008**, *321*, 821−823.
(11) Smith, O. L.; Kim, Y.; Kathaperumal, M.; Gadinski, M. R.; Pan, M.-J.; Wang, Q.; Perry, J. W. Enhanced Permittivity and Energy Density in Neat Poly(Vinylidene Fluoride-Trifluoroethylene-Chlorotrifluoroethylene) Terpolymer Films through Control of Morphology. *ACS Appl. Mater. Interfaces* **2014**, *6*, 9584−9589.
(12) Gregorio, R.; Botta, M. M. Effect of Crystallization Temperature on the Phase Transitions of P(VDF/TrFE) Copolymers. *J. Polym. Sci., Part B: Polym. Phys.* **1998**, *36*, 403−414.
(13) Bargain, F.; Panine, P.; Domingues Dos Santos, F.; Tencé-Girault, S. From Solvent-Cast to Annealed and Poled Poly(VDF-Co-TrFE) Films: New Insights on the Defective Ferroelectric Phase. *Polymer* **2016**, *105*, 144−156.
(14) Yagi, T.; Tatemoto, M.; Sako, J. Transition Behavior and Dielectric Properties in Trifluoroethylene and Vinylidene Fluoride Copolymers. *Polym. J.* **1980**, *12*, 209−223.
(15) Chung, T. C.; Petchsuk, A. Synthesis and Properties of Ferroelectric Fluoroterpolymers with Curie Transition at Ambient Temperature. *Macromolecules* **2002**, *35*, 7678−7684.
(16) Gadinski, M. R.; Li, Q.; Zhang, G.; Zhang, X.; Wang, Q. Understanding of Relaxor Ferroelectric Behavior of Poly(Vinylidene Fluoride−Trifluoroethylene−Chlorotrifluoroethylene) Terpolymers. *Macromolecules* **2015**, *48*, 2731−2739.
(17) Kassa, H. G.; Nougaret, L.; Cai, R.; Marrani, A.; Nysten, B.; Hu, Z.; Jonas, A. M. The Ferro- to Paraelectric Curie Transition of a Strongly Confined Ferroelectric Polymer. *Macromolecules* **2014**, *47*, 4711−4717.
(18) Serghei, A.; Zhao, W.; Miranda, D.; Russell, T. P. Curie Transitions for Attograms of Ferroelectric Polymers. *Nano Lett.* **2013**, *13*, 577−580.
(19) Lutkenhaus, J. L.; McEnnis, K.; Serghei, A.; Russell, T. P. Confinement Effects on Crystallization and Curie Transitions of Poly(Vinylidene Fluoride-Co-Trifluoroethylene). *Macromolecules* **2010**, *43*, 3844−3850.
(20) Hawker, C. J.; Russell, T. P. Block Copolymer Lithography: Merging "Bottom-Up" with "Top-Down" Processes. *MRS Bull.* **2005**, *30*, 952−966.
(21) Loo, Y.-L.; Register, R. A. Crystallization Within Block Copolymer Mesophases. In *Developments in Block Copolymer Science and Technology*; Wiley-Blackwell: 2004; pp 213−243.
(22) Michell, R. M.; Müller, A. J. Confined Crystallization of Polymeric Materials. *Prog. Polym. Sci.* **2016**, *54*−*55*, 183−213.
(23) Bates, F. S.; Fredrickson, G. H. Block Copolymers—Designer Soft Materials. *Phys. Today* **1999**, *52*, 32−38.
(24) Loo, Y.-L.; Register, R. A.; Ryan, A. J.; Dee, G. T. Polymer Crystallization Confined in One, Two, or Three Dimensions. *Macromolecules* **2001**, *34*, 8968−8977.
(25) Voet, V. S. D.; Tichelaar, M.; Tanase, S.; Mittelmeijer-Hazeleger, M. C.; ten Brinke, G.; Loos, K. Poly(Vinylidene Fluoride)/Nickel Nanocomposites from Semicrystalline Block Copolymer Precursors. *Nanoscale* **2013**, *5*, 184−192.
(26) Meereboer, N. L.; Terzić, I.; Saidi, S.; Hermida Merino, D.; Loos, K. Nanoconfinement-Induced β-Phase Formation Inside Poly(Vinylidene Fluoride)-Based Block Copolymers. *ACS Macro Lett.* **2018**, *7*, 863−867.
(27) Voet, V. S. D.; Hermida-Merino, D.; ten Brinke, G.; Loos, K. Block Copolymer Route towards Poly(Vinylidene Fluoride)/Poly-(Methacrylic Acid)/Nickel Nanocomposites. *RSC Adv.* **2013**, *3*, 7938−7946.
(28) Terzić, I.; Meereboer, N. L.; Loos, K. CuAAC Click Chemistry: A Versatile Approach towards PVDF-Based Block Copolymers. *Polym. Chem.* **2018**, *9*, 3714−3720.
(29) Voet, V. S. D.; Alberda van Ekenstein, G. O. R.; Meereboer, N. L.; Hofman, A. H.; ten Brinke, G.; Loos, K. Double-Crystalline PLLA-b-PVDF-b-PLLA Triblock Copolymers: Preparation and Crystallization. *Polym. Chem.* **2014**, *5*, 2219−2230.
(30) Faber, M.; Hofman, A. H.; Loos, K.; ten Brinke, G. Highly Ordered Structure Formation in RAFT-Synthesized PtBOS-b-P4VP Diblock Copolymers. *Macromol. Rapid Commun.* **2016**, *37* (11), 911−919.
(31) Borsboom, M.; Bras, W.; Cerjak, I.; Detollenaere, D.; Glastra van Loon, D.; Goedtkindt, P.; Konijnenburg, M.; Lassing, P.; Levine, Y. K.; Munneke, B.; et al. The Dutch−Belgian Beamline at the ESRF. *J. Synchrotron Radiat.* **1998**, *5*, 518−520.
(32) Bras, W.; Dolbnya, I. P.; Detollenaere, D.; van Tol, R.; Malfois, M.; Greaves, G. N.; Ryan, A. J.; Heeley, E. Recent Experiments on a Small-Angle/Wide-Angle X-Ray Scattering Beam Line at the ESRF. *J. Appl. Crystallogr.* **2003**, *36*, 791−794.
(33) Michell, R. M.; Blaszczyk-Lezak, I.; Mijangos, C.; Müller, A. J. Confinement Effects on Polymer Crystallization: From Droplets to Alumina Nanopores. *Polymer* **2013**, *54*, 4059−4077.
(34) Ho, V.; Boudouris, B. W.; McCulloch, B. L.; Shuttle, C. G.; Burkhardt, M.; Chabinyc, M. L.; Segalman, R. A. Poly(3-Alkylthiophene) Diblock Copolymers with Ordered Microstructures and Continuous Semiconducting Pathways. *J. Am. Chem. Soc.* **2011**, *133*, 9270−9273.
(35) Lin, M.-C.; Chen, H.-L.; Lin, W.-F.; Huang, P.-S.; Tsai, J.-C. Crystallization of Isotactic Polypropylene under the Spatial Confinement Templated by Block Copolymer Microdomains. *J. Phys. Chem. B* **2012**, *116*, 12357−12371.
(36) Kratochvíl, J.; Šturcová, A.; Sikora, A.; Dybal, J. Note on the Glass Transition Temperature of Poly(Vinylphenol). *Eur. Polym. J.* **2009**, *45* (6), 1851−1856.
(37) Bune, A. V.; Fridkin, V. M.; Ducharme, S.; Blinov, L. M.; Palto, S. P.; Sorokin, A. V.; Yudin, S. G.; Zlatkin, A. Two-Dimensional Ferroelectric Films. *Nature* **1998**, *391*, 874−877.

DOI: 10.1021/acs.macromol.8b02382
Macromolecules 2019, 52, 1567−1576

(38) Teyssedre, G.; Bernes, A.; Lacabanne, C. Cooperative Movements Associated with the Curie Transition in P(VDF-TrFE) Copolymers. *J. Polym. Sci., Part B: Polym. Phys.* **1995**, *33* (6), 879−890.
(39) Chen, G.; Wang, X.; Lin, J.; Yang, W.; Li, H.; Wen, Y. Interfacial Polarity Modulation of KTa0.5Nb0.5O3 Nanoparticles and Its Effect on Dielectric Loss and Breakdown Strength of Poly-(Vinylidene Fluoride) Nanocomposites with High Permittivity. *J. Phys. Chem. C* **2016**, *120*, 28423−28431.
(40) Zhou, T.; Zha, J.-W.; Cui, R.-Y.; Fan, B.-H.; Yuan, J.-K.; Dang, Z.-M. Improving Dielectric Properties of BaTiO3/Ferroelectric Polymer Composites by Employing Surface Hydroxylated BaTiO3 Nanoparticles. *ACS Appl. Mater. Interfaces* **2011**, *3* (7), 2184−2188.
(41) Dai, Z.-H.; Han, J.-R.; Gao, Y.; Xu, J.; He, J.; Guo, B.-H. Increased Dielectric Permittivity of Poly(Vinylidene Fluoride-Co-Chlorotrifluoroethylene) Nanocomposites by Coating BaTiO3 with Functional Groups Owning High Bond Dipole Moment. *Colloids Surf., A* **2017**, *529*, 560−570.
(42) Prateek; Thakur, V. K.; Gupta, R. K. Recent Progress on Ferroelectric Polymer-Based Nanocomposites for High Energy Density Capacitors: Synthesis, Dielectric Properties, and Future Aspects. *Chem. Rev.* **2016**, *116* (7), 4260−4317.
(43) Singh, D.; Choudhary, A.; Garg, A. Flexible and Robust Piezoelectric Polymer Nanocomposites Based Energy Harvesters. *ACS Appl. Mater. Interfaces* **2018**, *10* (3), 2793−2800.
(44) Faber, M.; Hofman, A. H.; Loos, K.; ten Brinke, G. Highly Ordered Structure Formation in RAFT-Synthesized PtBOS-b-P4VP Diblock Copolymers. *Macromol. Rapid Commun.* **2016**, *37*, 911−919.

DOI: 10.1021/acs.macromol.8b02382
Macromolecules 2019, 52, 1567−1576